APPENDIX I

# APPENDIX-I

## EXTERNAL ENERGY LOSSES IN VIBRATING REED INTERNAL FRICTION EXPERIMENT :

We have already noted in the second chapter that during vibrating reed internal friction measurements external energy losses should be minimized to a sufficiently low level, in order to resolve the internal friction peaks (anelastic relaxations). For the sake of completeness, in this appendix, we give a brief account about these losses, as reported earlier[1]. There exists four main types of external energy losses viz. air damping, transducer losses and specimen support losses and transverse thermal current losses. The motion of air damping primarily refers to the loss of energy of vibrating reed due to frictional forces offered by air molecules. At normal pressures, this energy loss is much greater than that of the internal friction[(1)]. To get some feeling about air damping we have reproduced here the data on nature of damping behaviour of silica reed at different background pressures as also for different tones of vibrations[(1)]. Fig.1. shows the variation of log-decrement as a function of background air pressure and tones of vibrations. Although the principle features of this variation are similar, the actual values of log-decrement at a given background pressure vary and is different for different tones of vibrations. As shown in Fig.1, above pressures of approximately 0.1 Torr dependence of air damping is much

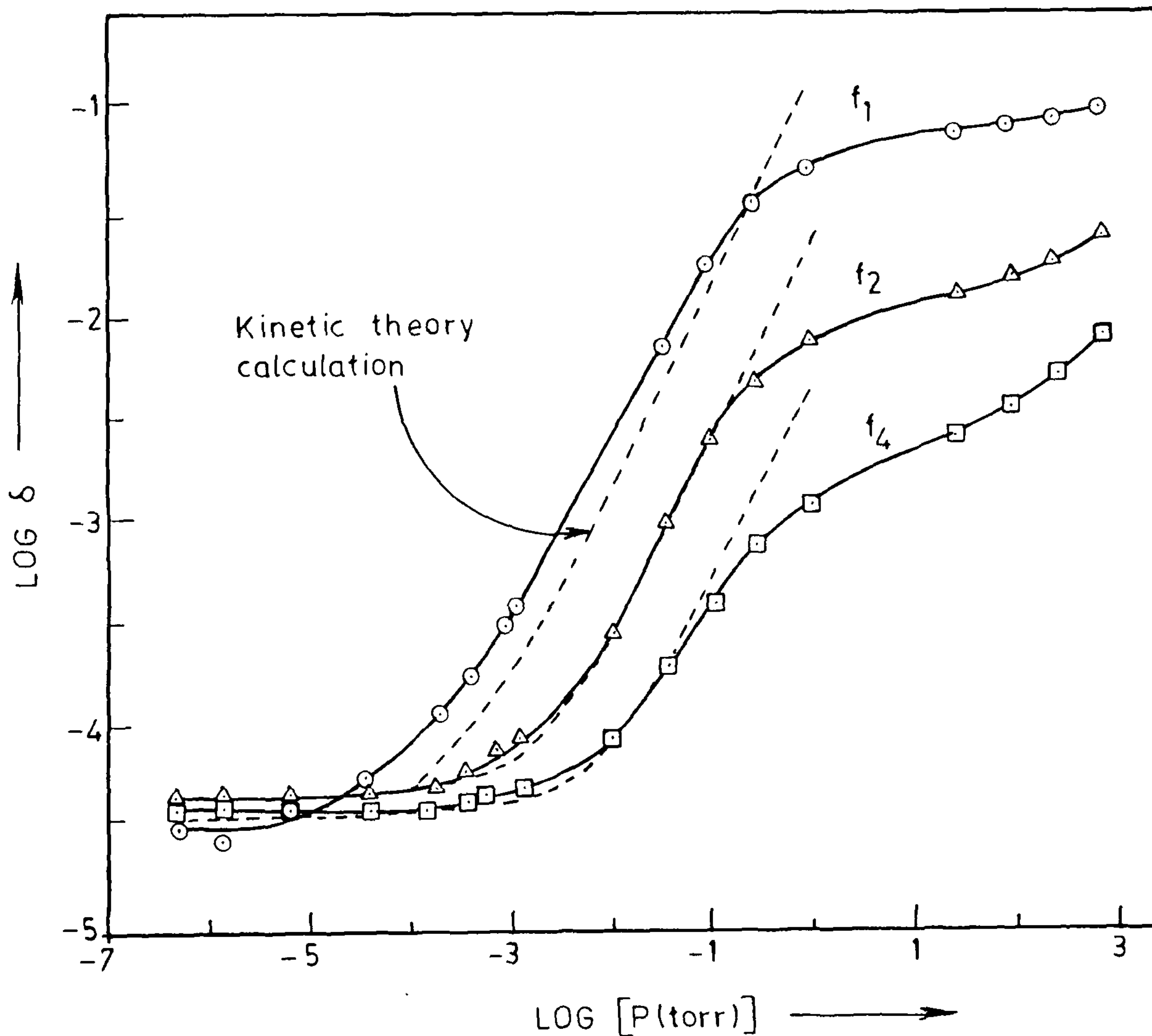


Fig. 1 Damping of a 50 μm thick fused silica reed with a 4500 Å Niobium film on each face of the reed as a function of air pressure[1]. The measurements were made at room temperature using first, second and fourth tones of vibration. The broken curves give the calculated air damping superimposed on the background internal friction of the sample.

less marked, however, below 0.1 Torr it is simply proportional to the pressure. This behaviour can be understood in terms of a transition from a viscous flow to a molecular flow condition. In the molecular flow region, these authors have calculated an amount of air damping. The calculations are based upon simple kinetic theory wherein air damping is given by the relation

$$\delta_A = 2P/f_n \rho\, d\bar{u}$$

where P is the air pressure, $\bar{u}$ is the average molecular velocity. $\rho$ and d are density and thickness of the reed specimen and $f_n$ is the frequency of the particular tone used. As depicted by the dotted curve, these calculations were found to be in a good agreement with the experiment in low pressure region. A final noteworthy point is that below a pressure of approximately $10^{-5}$ Torr, the value of air damping saturates and becomes constant for more lower pressures. It is thus clear that to minimise air damping during internal friction measurements, it is necessary to carry out the experiment in a vacuum better than $10^{-5}$ Torr.

Another important contribution to the external energy loss comes from the support where the reed specimen is clamped in a cantilever fashion. The support position of the reed specimen experiences maximum surface strain for all tones of vibrations. The independent assessment of this type of energy loss is not possible, however, if the reed specimen exhibits a log-decrement value of $10^{-4}$ in a background pressure of less than $10^{-5}$ Torr, it is an indication that the support losses are reduced to a very low level. The important factor in achieving such a low support loss is to eliminate mechanical slippage and rubbing friction at the root position of reed specimen. In this

context Berry[2] has suggested that forming the integral bound of reed specimen with pedestal support serves the purpose of the minimization of support losses. In the present case, we, however, have opted for mechanical clamping of reed specimen to the pedestal. This method of clamping offers difficulties in the case of thin reeds of brittle materials such as silicon and gallium arsenide. To overcome this, we have used a special method for sample preparation discussed in the second chapter.

The third category of energy losses is transducer loss. Since the detection mechanism employed is capacitive coupling one, transducer losses are bound to occur. These losses are associated with the capacitive network utilized in the circuit. The losses can be realized by considering a series circuit consisting of a capacitor C, a resistor R and a battery $V_b$. The capacitance C can then be said to be the sum of the individual capacitances $C_e$ and $C_s$, where $C_e$ is the capacitance formed between the electrode face and the grounded reed and $C_s$ is the stray capacitance of the wiring. The work done by the vibrating reed specimen in yielding a voltage $v_o$ across the resistance R enables one to find the transducer losses. If $\Delta W_T$ denotes the loss then

$$\Delta W_T = \left(\frac{\pi (C_e V_b a_o)^2}{C g^2}\right) \frac{\omega C R}{1 + (\omega C R)^2} \qquad \ldots 1$$

and

$$v_o = V_b \left(\frac{a_o C_e}{g C}\right) \frac{\omega C R}{(1 + (\omega C R)^2)^{1/2}} \qquad \ldots 2$$

where $\omega$ is the circular frequency, $a_o$ is the amplitude of the motion of the reed at the position of the detection electrode, g is the distance between the reed and the electrode. It can be seen from

inspection of the equation (1) and (2) that when $\omega\tau < 1$, the detection sensitivity falls off and it tends to a limiting asymptotic value for $\omega\tau > 1$. Also it can be seen that $\Delta W_T$ follows a classical Debye form, and reaches a maximum at $\omega\tau = 1$ and approaches zero asymptotically for both high and low frequency limits. The logarithmic decrement associated with the transducer loss is given by

$$\delta_T = \Delta W_T / K_n A_o^2$$

where $A_o$ is the amplitude of the motion at the free end of the reed and $K_n$ is the effective spring constant of the mode.

Fourth category of the energy loss is transverse thermal current loss and arises due to thermoelastic mechanism when the reed specimen is subjected to transverse vibration. This loss is relatively of lesser magnitude and simply contributes to the background damping level. The loss can be calculated from the expression

$$\delta_T = (\pi E \alpha^2 T / \rho S) f f_o / [1 + (f f_o)^2]$$

where E is Young's modulus, $\alpha$ is a linear expansion coefficient, T is the absolute temperature, $\rho$ is the density, S is the specific heat and f is the frequency of vibration of the reed. This type of loss is negligible in the case of material having low expansion behaviour. For example at room temperature this loss is small and increases with the increasing temperature.

REFERENCES

1. B.S. Berry and W.C. Pritchet : IBM, J. Res. Develop., 19(4), 334 (1975).

2. S.I. Tan, B.S. Berry and W.F.J. Frank, in Ion-Implantation in Semiconductors and other Materials, Edited by B.L. Crowder, Plenum Press Inc. New York, 19-30 (1973).

## APPENDIX-II

### ION-IMPLANTATION TECHNIQUE:

In this appendix we briefly give the basic features of ion-implantation technique. Ion implantation of solids basically refers to the irradiation of solid surface by energetic ion beam. The energy of ion beam typically lies in the range of few tens to a few hundreds of KeV. Owing to such a high energy, incident ion penetrates the solid surface and experiences a series of energy degrading collisions with the target atoms. The kinetic energy of the ion is thus rapidly deposited surrounding the ion track. Due to this deposited energy, target atoms are set into motion forming higher order collisions. Such sequential scattering events generate a zone in the neighbourhood of ion track in the solid which contains a large concentration of defects. This zone typically extends over a lateral dimension of approximately a few tens of Angstroms and is referred as a "collision cascade" zone. The collision cascade formation occurs over a time scale of $10^{-13}$-$10^{-10}$ sec and as such it renders highly non-equilibrium nature to ion beam processing. The immediate consequence of such a stir-up is to set up various kinds of solid state phenomena such as production of defects, defect complexes and agglomoration, sputtering of target atoms, radiation enhanced diffusion and segregation, dynamical mixing of atomic species etc. leading to the precipitation of unconventional compositional and structural features in the surface layers of the solid. The processed material, thus, can offer novel chemical and physical responses which can not be realised

via conventional equilibrium processing concepts such as furnace annealing.

When ions penetrate into solids via scattering events distributed statistically in space and time, they come to rest at different depths below the surface. In general, one obtains a semi-Gaussian distribution of ions as shown in Fig.1(a) with projected range $R_p$ and straggled range $\Delta R_p$ of a few hundreds Angstroms, where $\Delta R_p$ refers to the value of FWHM (Full Width at Half Maxima) of Gaussian distribution decided by $2(2 \ln 2)^{1/2}$. Under special circumstances wherein ions are incident on a crystalline solid along one of its low index crystallographic directions, non-standard range distributions can result due to ion-channelling effects Fig.1(b). Under these conditions, penetration depths as high as a micron can also be obtained. The defects or defect complexes produced by the ion can also led to some interesting variations of ion profiles from those obtained on the basis of simple ion-target considerations because their concentration profile may not follow the distribution of the dopant. The occurrence of such variations of ion-profiles can generally be attributed to the influence of defect assisted (or radiation enhanced) diffusion on the dopant redistribution, especially in the case of high dose implants. Fig.2 shows the results for $Ar^+$ ion implants in $SiO_2$ matrix at dose values of $1 \times 10^{15}$ and $1 \times 10^{16}$ ions/$cm^2$ represented by curves (a) and curve (b) respectively and obtained by using standard 'Suspre' Code.

In the present work we used the Ion-Implantation system designed and developed in our laboratory. In this system, the ions are produced in a diffused discharge type of ion source, and are then extracted by

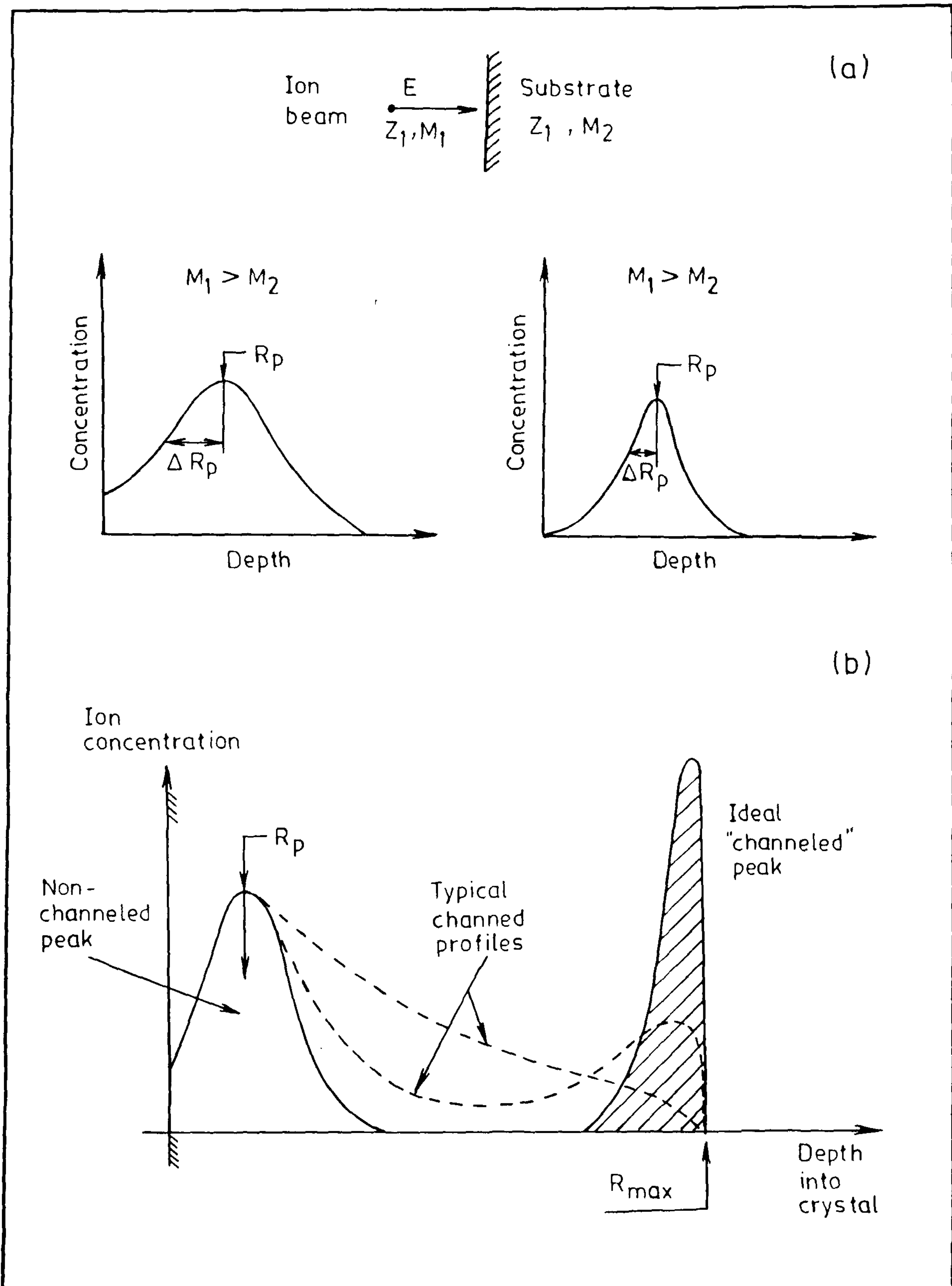


Fig. 1 Depth distribution of implanted ions (a) in an amorphous solid and (b) in a single crystal when the ions are incident along one of the low index crystallographic directions (channelling).

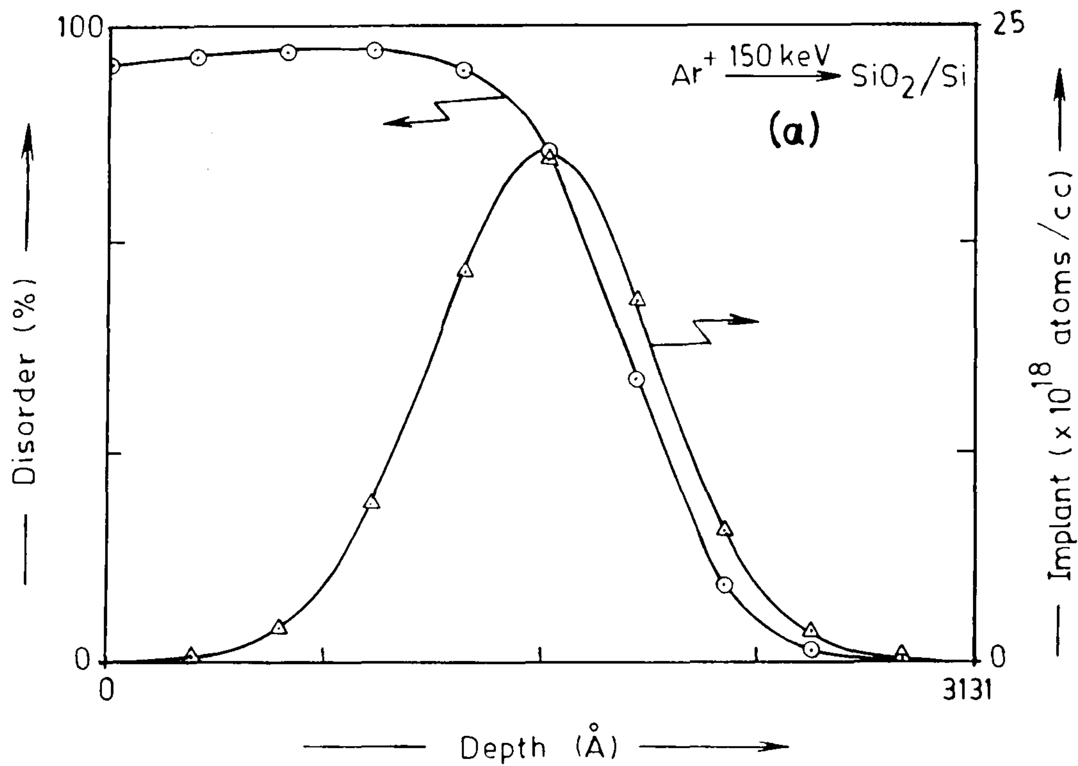


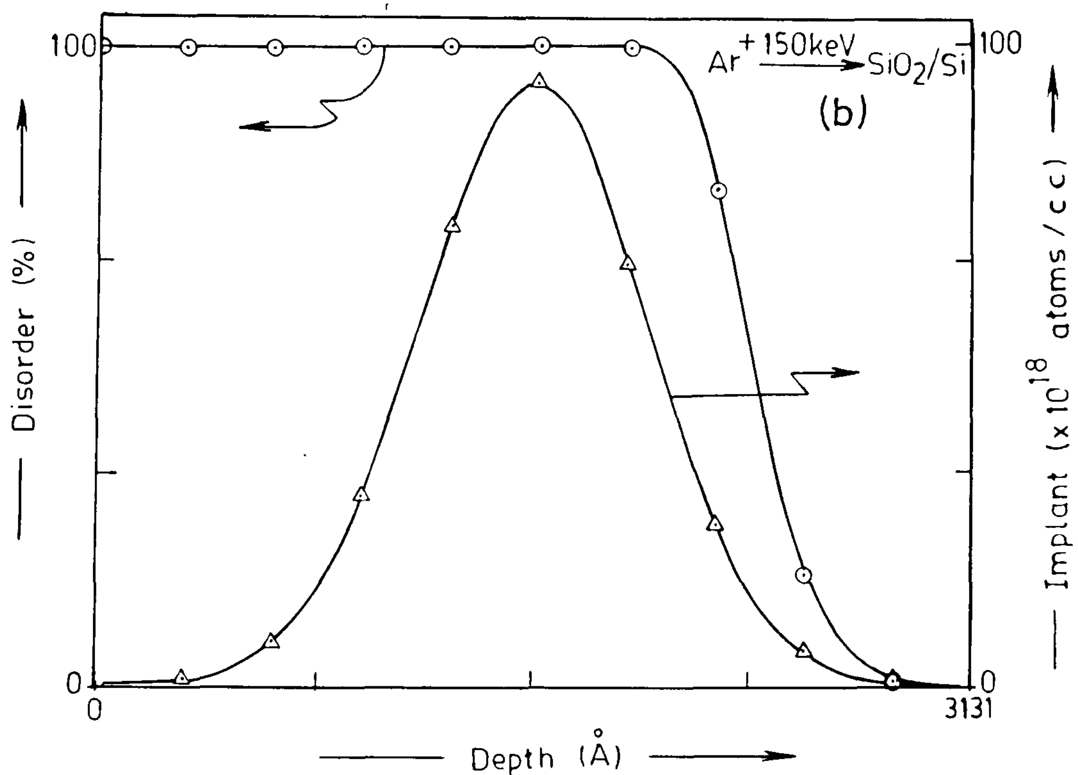


Fig. 2 Distribution of 150 KeV Argon atoms and amount of disorder in $SiO_2$ matrix at different dose values (a) 1 X $10^{15}$ $Ar^+/cm^2$ (b) 1 X $10^{16}$ $Ar^+/cm^2$

a suitable extraction geometry. The ion beam thus formed is focused by using an electrostatic Enziel Lens and then mass analysed by using 60$^{o}$ magnetic seperator. Mass selected beam is then energized to a desired energy (150 KeV) by using 15 stage accelerating column and is then made incident on the target kept in a target chamber. The beam size is of $\sim$ 5mm diameter and it is scanned all over the sample area by using an electrostatic sweeping mechanism. Dose measurement is carried out by precision electrometer and current integrator. During implantation the sample is surrounded by a cold trap to minimise any contamination. The implantation process is carried out in a background pressure of better than 1 X 10$^{-6}$ Torr.